Nanostructures

DOI: 10.1002/anie.200600429

Hierarchical Structured Nanohelices of ZnS**

*Daniel Moore, Yong Ding, and Zhong Lin Wang**

Wurtzite-structured materials, such as ZnO, ZnS, GaN, and AlN, have an important characteristic: the presence of polar surfaces that result from cation- or anion-terminated atomic planes. Consequently, a series of novel nanostructures, such as nanosprings,[1,2] nanorings,[3–5] nanohelices,[6] and nanobows,[7] have been formed. The mechanism that drives the formation of these novel configurations minimizes the electrostatic-interaction energy of the polar surfaces. As of now, these nanostructures have been mainly observed for ZnO, although nanosprings of wurtzite-structured AlN[5] and rutile-structured SnO_2[3] have also been observed as a result of the same formation mechanism.

ZnS, as another member in the wurtzite family and one of the most important materials in photonics, is a direct wide-band-gap (3.91 eV) semiconductor with a high index of refraction and a high transmittance in the visible range.[8–12] As for one-dimensional nanostructures, ZnS has been synthesized as nanowires, nanobelts, nanotubes, and nanocombs.[9,13–20] Recently, ZnS nanobelts have been doped with manganese, by post-annealing, without changing the crystallography of the ZnS nanobelts.[21] Optically pumped lasing has also been shown in single ZnS nanobelts.[22]

Herein, we report for the first time the high-yielding synthesis of hierarchical structured ZnS nanohelices. The morphology of the ZnS nanohelix is more complex than that observed for ZnO. The mechanism and the process of formation of the hierarchical structure are presented on the basis of the structural information provided by electron microscopy analysis. It is concluded that the hierarchical structure is a combined result of several growth features in the wurtzite ZnS.

The synthesis is based on the vapor deposition process. The as-synthesized samples were analyzed by using X-ray diffraction (XRD) and scanning electron microscopy. The XRD data confirmed that the as-synthesized sample was wurtzite ZnS. Optically, it appears yellow–white and covers the silicon deposition substrate. The synthesized material has a relatively high yield on the substrate and shows a high degree of reproducibility. The deposited material has a dominant morphology, which consists of helices of a ZnS

[*] D. Moore, Dr. Y. Ding, Dr. Z. L. Wang
Department of Materials science and Engineering
Georgia Institute of Technology
Atlanta, GA 30332-0245 (USA)
Fax: (+1) 404-894-8008
E-mail: zhong.wang@mse.gatech.edu

[**] We thank for the support from NSF, the NASA Vehicle Systems Program, Department of Defense Research and Engineering (DDR&E), and the Defense Advanced Research Projects Agency (Award No. N66001-04-1-8903).

WILEY InterScience DISCOVER SOMETHING GREAT
© 2006 Wiley-VCH Verlag GmbH & Co. KGaA, Weinheim

nanobelt. Some scanning electron microscopy (SEM) images of the sample are shown in Figure 1: As can be seen in Figure 1 a, the yield of the helical structures is rather high, and Figure 1 b shows a very long, densely branched nanohelix. The

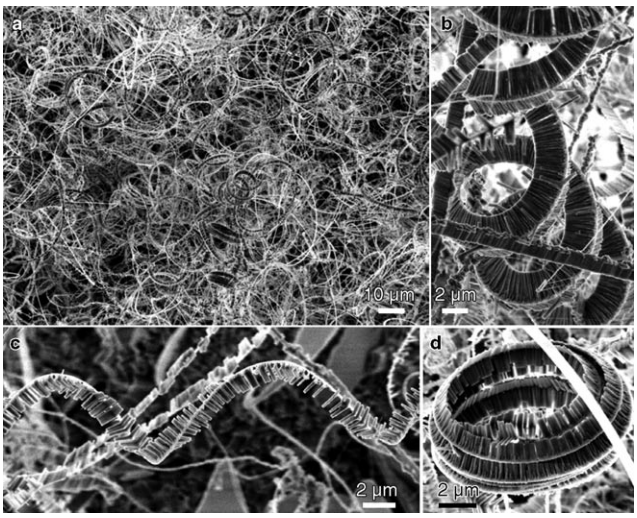

Figure 1. a) Low magnification SEM image that shows the high yield of ZnS nanohelices on the silicon substrate. b) A very long and densely branched nanohelix. c) A more typical moderately branched nanohelix. d) A densely branched nanohelix that has fallen in on itself and loosely formed a ringlike structure.

side branches align well and form an ordered structure along the entire length of the nanohelix. Figure 1 c shows a helix that is long and moderately branched, which is by far the most commonly observed ZnS nanohelix, though the others are common as well. Figure 1 d shows a helix that has curled up into itself to form a ringlike structure.

The nanohelices are made up of two parts: The first is the spine, which coils into a helical shape; the second has Y-shaped branches that all grow to the same size and at the same side of the spine in each nanohelix. The Y-branched structures always grow toward the inside of the helix (Figure 2 a), and they rotate and follow the curled shape of the nanohelix. The Y branches are densely packed to form an aligned and ordered array that follows the coiling geometry of the helix (Figure 2 b).

Statistical data were recorded a wide range of aspects of the helices. The analysis of nearly one hundred separated helices recorded the pitch, radius, and handedness of the helix. No direct relationship was found between pitch and radius, and no preferences towards handedness was noticed (of the helices that could be measured, about 60 % were right-handed and about 40 % left-handed).

The structure of the hierarchical nanohelix was analyzed by transmission electron microscopy (TEM) to understand the formation process. Figure 3 a shows a low-magnification TEM image of a segment of the nanohelix: The Y structure has two V-shaped branches that are rather smooth in shape, but the bottom branch connected to the spine is rather rough, thus possibly indicating some subsequent growth at the side surface (Figure 3 b). Figure 3 c and e are, respectively, a TEM

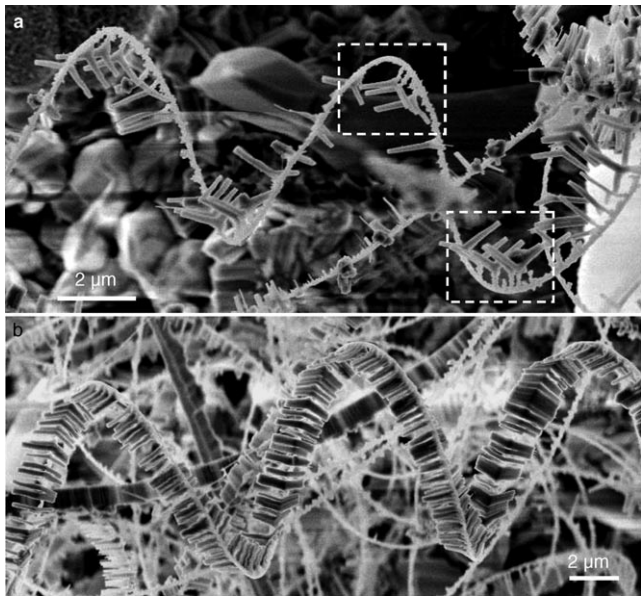

Figure 2. a) A lightly branched nanohelix. The branched secondary growth always grows towards the inside of the helix as seen particularly in the two boxed areas. The nanohelices consist of a spine which coils in a helical shape. On the inner side of the spine there is Y-shaped secondary growth which grows to the same length along an individual nanohelix. b) Another typical, moderately branched nanohelix. The Y-shaped branches always point towards the inside of the coil, regardless of the handedness of the nanohelix, thus suggesting that the inner face is the chemically active Zn-terminated face.

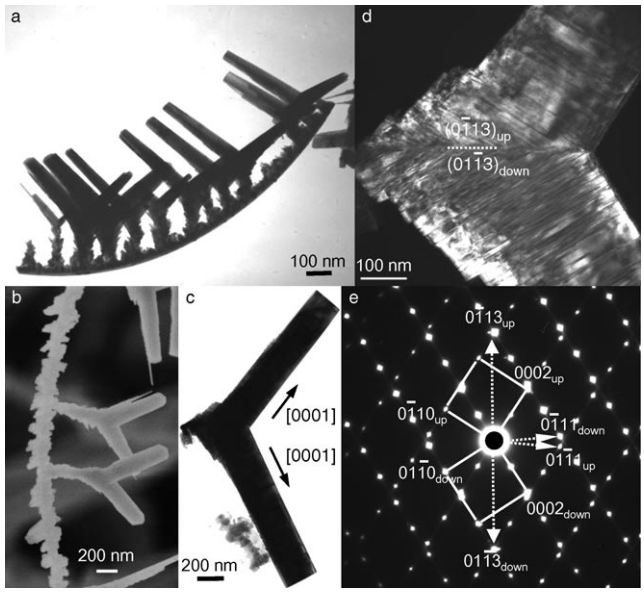

Figure 3. a) A typical TEM image of the ZnS nanohelix. It has been broken as a result of transfer from the silicon deposition substrate to the TEM sample holder. b) An SEM close-up of the secondary Y-shaped branches that grew towards the inside of the helix. The rough growth surface is visible. c) Top-down view of a typical branch growth, its selective-area electron-diffraction (SAED) pattern (e) shows the (0113) twin structure and the growth direction of the branch is along the [0002] direction. d) The dark-field image of the branch growth and the twin plane that reveals a large number of stacking faults, thus indicating a large amount of local strain in the crystal.

 © 2006 Wiley-VCH Verlag GmbH & Co. KGaA, Weinheim

image and the corresponding electron diffraction pattern recorded from the V branches with the incident electron beam perpendicular to the V plane. The V branches have a twin relationship, and the twin plane is $(0\bar{1}13)$, as previously observed for ZnO and CdSe.[23] The diffraction pattern is composed of two sets of diffraction spots that have a symmetrical geometrical layout. The common spot is the twin boundary plane $(0\bar{1}13)$ or $(01\bar{1}3)$. The incident beam direction, for example, the normal direction of the V-branch plane, is $[\bar{2}110]$. This behavior also indicates that the growth direction of the coiling spin is $[\bar{2}110]$. The growth directions of the two branches of the V-shaped structure are [0001]. The stacking faults that lie in the (0001) plane can be clearly seen in the two V branches, which are produced by the structural transformation between wurtzite and the zinc blend,[14] through the dark-field TEM image displayed in Figure 3d.

We next rotated the sample so that it was orientated with one side of the V branches parallel to the electron beam (Figure 4a). The corresponding electron diffraction pattern in

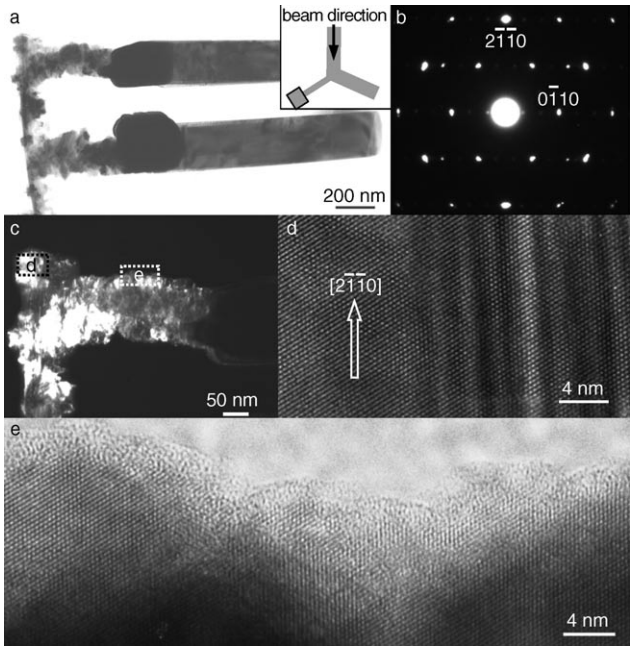

Figure 4. a) A bright-field TEM image with the beam direction along the length of one of the secondary growth branches (inset). b) The SAED pattern of the spine, which shows the growth plane of the spine is the $(2\bar{1}\bar{1}0)$ plane. c) Dark-field image that highlights the growth of the spine and the branched growth. A high-resolution image of d) the spine of the nanohelix and e) the rough secondary growth.

Figure 4b is dominated by the [0001] pattern with some extra spots contributed by the other side branch of the V structure. A dark-field TEM image using one of the diffraction spot shows that the nanohelical spine is a single-crystal piece with one branch of the V structure, although its surface is rough. A high-resolution TEM (HRTEM) image recorded from the selected area d (Figure 4c) clearly display the structure of wurtzite ZnS projected along the *c* axis (Figure 4d). The growth direction of the spine is $[\bar{2}110]$. The HRTEM image (Figure 4e) recorded from the area e (Figure 4c) shows an identical structure as the spine, thus clearly indicating that the bottom branch of the Y structure is a single crystalline piece that belongs to the spine.

The structure of the hierarchical structure can be described as follows (Figure 5a): The spine grows along the

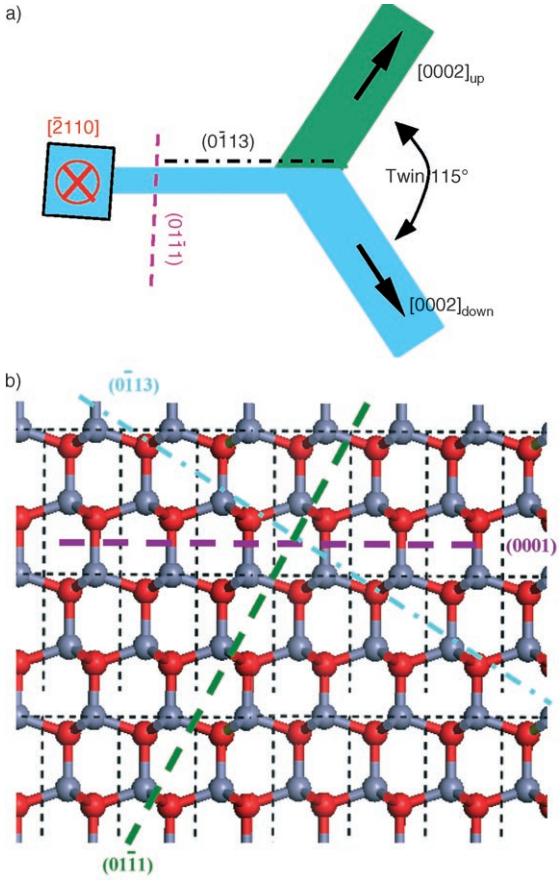

Figure 5. a) A schematic representation of the various planes and growth directions of the nanohelix. The main spine of the nanohelix is oriented along the $(2\bar{1}\bar{1}0)$ plane, with the polar $(01\bar{1}1)$ plane towards the inside of the helix. Off of this polar plane, the secondary growth occurs. b) A projection of the ZnS wurtzite lattice along the $(2\text{-}1\bar{1}0)$ plane that shows the key planes. The {0001} and $\{01\bar{1}1\}$ plane families are polar as they terminate with Zn^{+} and S^{-1} ions. The $\{0\bar{1}13\}$ plane is also shown, as it is the side plane of the initial secondary growth off the nanohelix.

$[\bar{2}110]$ direction, and its side surfaces are defined by $\pm(0\bar{1}13)$ and $\pm(01\bar{1}1)$. The surface is rough because the $\pm(0\bar{1}13)$ are higher energy planes. On the $(01\bar{1}1)$ surface, one branch grows out along $\approx[07\bar{7}4]$, a direction approximately perpendicular to the $(01\bar{1}1)$ plane. Then, a turn in growth direction from $\approx[07\bar{7}4]$ to [0002] leads to the formation of one of the V branches, and a twin growth by sharing the $(01\bar{1}3)$ plane results in the growth of the other branch. This change from the $[07\bar{7}4]$ growth direction to the [0002] direction occurs because of the very high energy associated with growth along the $[07\bar{7}4]$ direction. The direction [0002] is the fastest growth and lowest energy for wurtzite ZnS.

The nature of the $\{01\bar{1}1\}$ and $(0\bar{1}13)$ planes can be understood from the atomic model of ZnS. By projecting

 © 2006 Wiley-VCH Verlag GmbH & Co. KGaA, Weinheim

the structural unit cell along the $[\bar{2}110]$ direction, beside the most typical $\pm(0001)$ polar surfaces that are terminated with zinc and oxygen centers, respectively, the $\pm(01\bar{1}1)$ planes are also polar surfaces (Figure 5b). If $(01\bar{1}1)$ is terminated with zinc cations, the $(0\bar{1}1\bar{1})$ surface is terminated with sulfur anions, thus, the two surfaces will be positively and negatively charged, respectively.

The formation of the hierarchical structure can be separated into two major stages. The first stage is a fast growth of the spine defined by the $\{01\bar{1}1\}$ and $(01\bar{1}3)$ planes. The spine is confined by two oppositely charged zinc-terminated $(01\bar{1}1)$ and sulfur-terminated $(0\bar{1}1\bar{1})$ surfaces, and it can be viewed as a thin plate capacitor with a dipole moment across its width.[2] From our previous study on nanosprings and nanohelices of wurtzite ZnO,[1] the elastic deformation energy is rather small when the thickness of a nanobelt is small; thus, forming a circular structure would reduce the dipole moment of the nanobelt and minimize the energy contributed by the electrostatic interaction from the dipole-polarization and elastic deformation.[4] As a result, the nanobelt coils as the growth proceeds and forms the spine, thus resulting in the formation of a spring or helix with the $(01\bar{1}1)$ polar surface that face inward towards the coiling axis.

On the other hand, we know that the zinc-terminated surface is catalytically active and can induce secondary growth, whereas the sulfur-terminated surface is inert.[13] Thus, the side branches on the zinc-terminated $(01\bar{1}1)$ surface grow out, similar to the growth of the one-sided teeth of the ZnS nanocombs.[14] As described in Figure 5a, a switch and split in growth direction and a formation of a twin form the Y-branched structures. Moreover, the sulfur-terminated $(0\bar{1}1\bar{1})$ surface is inactive and shows no secondary growth. Therefore, the Y branches are aligned on one side of the spine (or nanobelt) and rotate according to the coiling shape of the spine, as observed in Figure 2.

As shown in Figures 1 and 2, the Y branches always point inward to the center. An alternative explanation is that the zinc-terminated $(01\bar{1}1)$ surface may have a larger stress than the sulfur-terminated $(0\bar{1}1\bar{1})$ surface, thus resulting in one-directional bending of the nanobelt. This process can co-contribute to the formation of the nanohelix, which may be a case for ZnS, but our previous study shows that this process is not the dominant for ZnO in the formation of nanosprings.[24]

In summary, hierarchical nanohelices of ZnS are reported for the first time. The nanohelices were synthesized by a vapor deposition process at high yield. The hierarchical nanohelix is formed by a combination of several growth characteristics for the wurtzite structure. The spine is a fast-growing nanobelt that is dominated by the $\pm(01\bar{1}1)$ polar and the $\pm(0\bar{1}13)$ nonpolar surfaces. The presence of polar surfaces results in coiling of the nanobelt to form a helix that minimizes the energy contributed by the polar charges to the surfaces. The difference in surface stress may also contribute to this process. The growth of the nanobelt/spine occurs rather fast. Then, the zinc-terminated $(01\bar{1}1)$ surface initiates the growth of one-sided teeth as a result of self-catalysis, similar to the nanocomb. Along the teeth, a switch in the growth-front plane from $(01\bar{1}1)$ to (0001) to lower the surface energy produces one branch of the Y structure. Finally, a $(0\bar{1}13)$ twin is formed at the switching point of the branch, thus resulting in the growth of the other branch along the [0001] direction, thus finally completing the Y structure. The twin is favorable as a result of the two possible phases of ZnS that coexist in the growth: the wurtzite hexagonal structure and zinc-blend cubic structure. The reported hierarchical nanohelices of ZnS could have novel mechanical, optical, and electrical properties.

Experimental Section

The synthesis of the ZnS nanohelices was carried out by using a simple vapor deposition process. Commercially available ZnS powder (Alfa Aesar, 99.99% purity, metal basis) was placed in the center of a single-zone horizontal tube furnace (Thermolyne 79300), in which the temperature, pressure, atmosphere, and evaporation time were controlled. Single-crystal silicon substrates with 1.5 nm of Au deposited on them with a thermal evaporator were placed "downstream" and at a lower temperature region in the furnace. These were used to collect the deposited material. Using a rotary vacuum pump, the tube was placed under vacuum for several hours to purge oxygen from the chamber. After evacuation to a pressure of about 2×10^{-3} Torr, the temperature in the center of the tube was elevated to 1000 °C at a rate of 50 °C min^{-1}. A N_2 gas flow was introduced into the system at a rate of 50 cm^2 min^{-1}. The inert N_2 gas acted as a carrier for transporting the sublimated vapor to cooler regions within the tube furnace for deposition onto the silicon substrates and also to help increase the pressure. The pressure was allowed to increase to a value of 20 Torr (about 25 mbar). The silicon substrates reached a temperature of about 750 °C. During evaporation, the products were deposited onto the silicon substrates. After maintaining these conditions for 2 h, the nitrogen gas flow was turned off and the products placed under vacuum. At this time, the furnace was allowed to cool to room temperature. The gold particle introduced initially was not found in the grown product, may be as a result of the vaporization of the gold at the early stage of the long growth (2 h).

Received: February 1, 2006
Published online: July 9, 2006

Keywords: chemical vapor deposition · nanohelices · nanostructures · sulfur · zinc

[1] X. Y. Kong, Z. L. Wang, *Nano Lett.* **2003**, *3*, 1625.
[2] R. Yang, Y. Ding, Z. L. Wang, *Nano Lett.* **2004**, *4*, 1309.
[3] R. Yang, Z. L. Wang, *J. Am. Chem. Soc.* **2006**, *128*, 1466.
[4] X. Y. Kong, Y. Ding, R. Yang, Z. L. Wang, *Science* **2004**, *303*, 1348.
[5] J. Duan, S. Yang, H. Liu, J. Gong, H. Huang, X. Zhao, J. Tang, R. Zhang, Y. Du, *J. Cryst. Growth* **2005**, *283*, 291.
[6] P. Gao, Y. Ding, W. Mai, W. Hughes, C. Lao, Z. L. Wang, *Science* **2005**, *309*, 1700.
[7] W. Hughes, Z. L. Wang, *J. Am. Chem. Soc.* **2004**, *126*, 6703.
[8] T. W. Odom, J. Henzie, Y. Babayan, E. C. Greyson, E. S. Kwak, *Talanta* **2005**, *67*, 507.
[9] Y. C. Zhu, Y. Bando, D. F. Xue, D. Golberg, *Adv. Mater.* **2004**, *16*, 831.
[10] R. A. Rosenberg, G. K. Shenoy, F. Heigl, S.-T. Lee, P.-S. G. Kim, X.-T. Zhou, T. K. Sham, *Appl. Phys. Lett.* **2005**, *86*, 263115.
[11] Y. W. Wang, L. D. Zhang, C. H. Liang, G. Z. Wang, X. S. Peng, *Chem. Phys. Lett.* **2002**, *357*, 314.
[12] J. S. Steckel, J. P. Zimmer, S. Coe-Sullivan, N. E. Stott, V. Bulovi, M. G. Bawendi, *Angew. Chem.* **2004**, *116*, 2206; *Angew. Chem. Int. Ed.* **2004**, *43*, 2154.

 © 2006 Wiley-VCH Verlag GmbH & Co. KGaA, Weinheim

[13] D. Moore, C. Ronning, C. Ma, Z. L. Wang, *Chem. Phys. Lett.* **2004**, *385*, 8.
[14] C. Ma, D. Moore, J. Li, Z. L. Wang, *Adv. Mater.* **2003**, *15*, 228.
[15] C. J. Barrelet, Y. Wu, D. C. Bell, C. Lieber, *J. Am. Chem. Soc.* **2003**, *125*, 11498.
[16] P. V. Radovanovic, C. J. Barrelet, S. Gradecak, F. Qian, C. Lieber, *Nano Lett.* **2005**, *5*, 1407.
[17] X. M. Meng, J. Liu, Y. Jiang, W. W. Chen, C. S. Lee, I. Bello, S. T. Lee, *Chem. Phys. Lett.* **2003**, *382*, 434.
[18] Y. Jiang, X. Meng, J. Liu, Z. Xie, C. S. Lee, S.-T. Lee, *Adv. Mater.* **2003**, *15*, 323.
[19] X. Fan, X.-M. Meng, X.-H. Zhang, W.-S. Shi, W.-J. Zhang, J. A. Zapien, C.-S. Lee, S.-T. Lee, *Angew. Chem.* **2006**, *118*, 2630; *Angew. Chem. Int. Ed.* **2006**, *45*, 2568.
[20] J. Hu, Y. Bando, J. Zhan, D. Golberg, *Angew. Chem.* **2004**, *116*, 4706; *Angew. Chem. Int. Ed.* **2004**, *43*, 4606.
[21] Y. Q. Li, J. A. Zapien, Y. Y. Shan, Y. K. Liu, S.-T. Lee, *Appl. Phys. Lett.* **2006**, *88*, 013115.
[22] J. A. Zapien, Y. Jiang, X. M. Meng, W. Chen, F. C. K. Au, Y. Lifshitz, S. T. Lee, *Appl. Phys. Lett.* **2004**, *84*, 1189.
[23] Y. Ding, Z. L. Wang, *J. Phys. Chem. B* **2004**, *108*, 12280.
[24] P. Gao, Z. L. Wang, *Small* **2005**, *1*, 945.

 © 2006 Wiley-VCH Verlag GmbH & Co. KGaA, Weinheim